3D Imaging With Moving Fringe Structured Illumination Microscopy

Alexandr Melnikov and Daniel P.-K. Lun, *Senior Member, IEEE*

***Abstract*—Structured Light Illumination Microscopy (SIM) has proved itself as a very effective method to improve the resolution of a widefield (WF) fluorescent microscope. In this paper, we demonstrate a new approach to three-dimensional (3D) imaging with the SIM, using a moving fringe (MF) illumination pattern. Instead of the standard three-beam standing wave illumination pattern, our method requires a two-beam one, varying along the optical axis. Each axial layer of the MF illumination pattern contains single-spatial-frequency interference fringes, traversing the space with its own speed (temporal frequency), proportional to the axial offset of such layer from the excitation plane. The different axial layers of a fluorescent object, excited with the MF illumination, will emit a continuous amplitude modulated fluorescent signal with the frequency of modulation proportional to the temporal frequency of the moving fringe pattern. The fine 3D image reconstruction is achieved via extracting the spatial location of the fluorescent object from the temporal frequency of amplitude modulated signal emitted by it. Since in our approach the problem of 3D image reconstruction is reduced to the problem of accurate temporal frequency estimation, any of the well-known spectrum estimation techniques can be applied to the problem, allowing the axial resolution improvement far beyond the limits of the classical 3D SIM. In this research, we suggest using the Minimum-norm method for the proposed MF SIM system, which gives a superior resolving power in spectrum estimation. Simulation results show that such a simple and rapid hardware implementation in combination with a straightforward signal processing method can, however, deliver an improvement in axial resolution far beyond the classical 3D SIM approach.**

***Index Terms*—Super-resolution 3D imaging, structural light illumination, Minimum-norm spectrum estimation.**

I. Introduction

STRUCTURED Light Illumination Microscopy (SIM) has proved itself as a very effective method to improve the lateral resolution of a widefield (WF) fluorescent microscope. This involves projecting a fine fringe pattern, which acts as a spatial carrier on the sample. This pattern downconverts the high-frequency components of the sample into the bandwidth of the optical system, allowing the reconstruction of a high-resolution image [1], [2].

Manuscript received March 10, 2022; revised March 30, 2022; accepted April 6, 2022. Date of publication April 12, 2022; date of current version April 26, 2022. This work was supported in part by the Research Grants Council of Hong Kong through Alexandr Melnikov's Ph.D. Fellowship Grant and in part by GRF under Grant 152478/16E. *(Corresponding author: Daniel P.-K. Lun.)*

The authors are with the Department of Electronic and Information Engineering, The Hong Kong Polytechnic University, Hong Kong SAR, China (e-mail: alex.melnikov@connect.polyu.hk; pak.kong.lun@polyu.edu.hk).

Digital Object Identifier 10.1109/JPHOT.2022.3166630

The early research works dedicated to SIM were focused on using intensity patterns with either lateral or axial periodicity. It has been demonstrated that the use of the laterally varying two-dimensional (2D) illumination patterns can lead either to lateral [1]–[4] or axial [5], [6] resolution improvement, but with no or limited effect on the other dimension. Similarly, it has been shown that axially varying fringe pattern can be used to enhance axial resolution only [7]. Both axial and lateral resolution can be enhanced simultaneously, but to do this, an illumination pattern with three-dimensional (3D) periodicity is required. 3D resolution doubling has been successfully achieved by interfering three mutually coherent illumination beams (further 3D SIM) [8].

All the methods above can deliver improvement in resolving capability of a fluorescent widefield microscope. However, since in these methods the structured light is projected on the sample using illumination optics, the spatial frequencies of the fringe pattern are restricted. The bandwidth of the final image with extended resolution remains a function of the illumination and imaging optics bandwidth, essentially limiting the improvement factor to two.

The direction of the future research works in SIM took a path of increasing complexity of the microscopy architecture in order to overcome the limiting effect of the restricted spatial frequencies of the fringe pattern. 3D SIM with dual objective lens is one such example [9] and 3D image reconstruction methods, based on subtractive SIM [10], [11] is another one. More advanced ways of phase information retrieval [12] and use [13] were also reported, as well as different combinations of SIM with other methods, like interferometry [14] and light-sheet microscopy [15].

A simple and elegant solution, allowing to bypass the limiting effect of the imaging optics in SIM, is to use a proximity projection grating to create structured light. In this case, no optical components are needed for projecting the fringe pattern on the sample, and hence, the spatial frequencies of the illumination pattern are not restricted anymore. Therefore, an improvement factor way beyond twofold can be achieved without paying a high price in terms of the complexity of the microscope architecture. This concept was successfully illustrated in [16], where the lateral resolution has been extended by a factor of four. However, the approach does not consider axial resolution improvement.

In the current work, we investigate the way of extending the axial resolution, in which the degree of improvement depends on the structured illumination only, but not on the imaging optics. Our method (further - Moving Fringe SIM) is based on the use

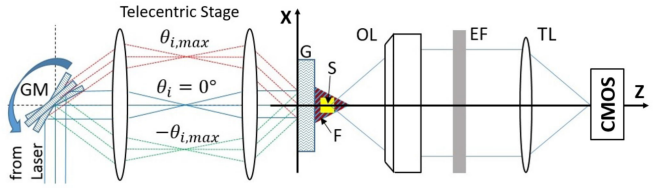

Fig. 1. Moving Fringe SIM system set up. GM–galvo-mirror; G–grating ($d = 833\,nm$); S sample; F fringes; EF – emission filter; TL - tube lens; OL – objective lens ($NA = 0.65$; $\Delta z_{WF} = 1.32\,\mu m$ at $\lambda_{em} = 559\,nm$; medium between the grating and the sample is the air ($n_m = 1$).

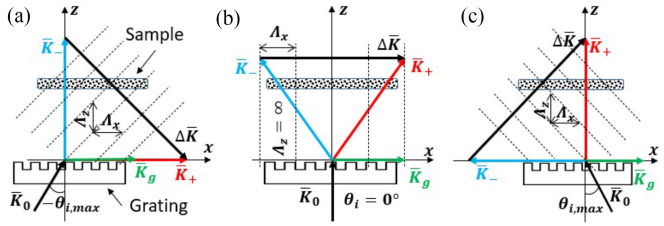

Fig. 2. Fringe pattern, formed by two first diffraction orders, produced by grating in response to tilted illumination at $\theta_i = -\theta_{i,max}$ (a); $\theta_i = 0$ (b); $\theta_i = \theta_{i,max}$ (c). $\overline{K}_0$ is a wave vector of tilted illumination; $\overline{K}_g$ is a grating vector; $\overline{K}_+$ and $\overline{K}_-$ are the first order wave vectors respectively; Λ_X and Λ_Z are fringe x- and z-periods respectively; black dashed line indicates fringes spatial orientation.

of the same proximity projection grating structure as in [16]. The major difference from the mentioned work is we focus on axial resolution improvement. Besides, we restrict the number of diffraction orders and operate in the far filed, rather than in the Fresnel region, shifting the fringes across the sample by more than just a single period with the step size smaller than one period. To our knowledge, no theoretical discussions or practical demonstrations of this method in application to the axial resolution enhancement have been published.

We create a 3D varying fringe pattern using only two light beams and a single rotary actuator to retrieve the information about the spatial structure of the sample. Targeting the axial resolution improvement, we do not consider the fringe pattern as a spatial carrier (unlike classical SIM), but it rather serves as an amplitude modulated excitation signal for the fluorophores. Application of the powerful data-adaptive spectrum estimation technique (such as the Minimum-norm estimator [17]) further improves the axial resolution of the Moving Fringe system well beyond the factor of two.

Thus, the Moving Fringe SIM, while maintaining a very simple microscope configuration, still can deliver a result comparable with much more complex and expensive systems, such as 4Pi or I ^{5} M, though. The ability to do a 3D image reconstruction with optical sectioning at nano-scale level and the improvement over the traditional 3D SIM method in axial resolution enhancement are demonstrated in our simulation. A proof-of-concept experiment is also conducted to test the imaging potential of the system.

For the sake of completeness, we also show in the Appendix that the classical 2D SIM approach still applies to the Moving Fringe system data, and it can be used to improve the lateral resolution of the system as well. The potential for combining these two approaches for a multidimensional super-resolution image reconstruction is briefly discussed.

II. Moving Fringe SIM

In this paper, we propose a new SIM structure that focuses on the improvement of axial resolution in 3D imaging. Fig. 1 shows a schematic diagram of the proposed Moving Fringe SIM system. As shown in the figure, a galvo-mirror is used to deflect the collimated light beam coming from the laser. The light beam varies in the $x - z$ plane only. The two lenses making the telecentric stage capture the deflected light and project it onto a grating structure. In response, a fine 1D transmission grating produces three diffraction orders, and their interference creates a fringe pattern, illuminating the sample. The spatial orientation of the interference fringes depends on the incident angle of the beam, illuminating the grating.

A fluorescent sample excited with the structured illumination emits light following the excitation pattern of the structured illumination but at a different wavelength. The light emitted by the sample is captured by the imaging optics and recorded by a CMOS camera. The excitation light, however, is blocked by the emission filter and thus will not affect the recorded image.

Fig. 2 illustrates how the fringe wave vector ΔK, produced by interfering diffraction orders, changes its spatial orientation depending on the incident angle (θ_i) of the illumination beam. At the moment we are going to focus on the interference signal between the two first order diffracted beams, as these two are of the main interest for our system. We will briefly discuss the effect of the interference between the zero order and first orders later.

For the given grating period (d), ΔK_x component of the fringe wave vector remains constant, following the grating equation: $\Delta K_x = 2K_g = 4\pi/d$. The ΔK_z component, however, changes with the change of the incident illumination angle:

$$\Delta K_z(\theta_i) = \frac{2\pi}{\lambda}\left(\sqrt{n_m^2 - \left[\sin\theta_i + \frac{\lambda}{d}\right]^2} - \sqrt{n_m^2 - \left[\sin\theta_i - \frac{\lambda}{d}\right]^2}\right) = \frac{2\pi}{\lambda}\beta(\theta_i), \quad (1)$$

where n_m is a refractive index of the medium behind the grating. The $\beta(\theta_i)$ parameter (also known as direction cosine [18]) is used for a more compact notation of the axial component of the fringe wave vector. When all the other parameters - wavelength, refractive index and the grating period - are fixed, the intensity of the fringe pattern, created by interference of the first order diffracted beams, at some point in space with $[x, z]$ coordinates, defined with respect to the grating plane and the optical axis, depends only on the instantaneous illumination angle θ_i as follows:

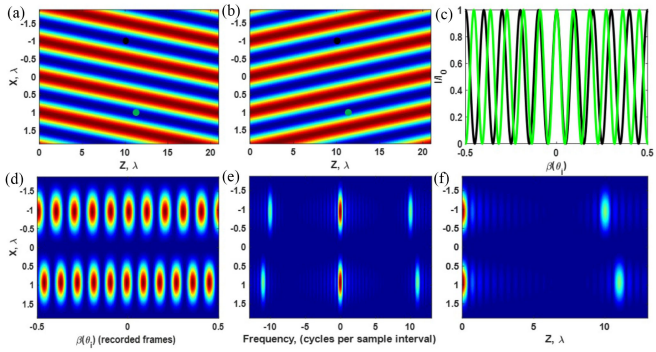

Fig. 3. 3D image reconstruction from prerecorded image stack using Fourier transform (black dot - fluorophore at $z_1 = 10\lambda$, green dot - fluorophore at $z_2 = 11\lambda$). (a) Fringe pattern orientation at $-\theta_i$. (b) Fringe pattern orientation at $+\theta_i$. (c) Illumination profile, seeing by fluorophores, as the fringe pattern moves, following the shift in incident illumination angle. Note that the profiles for the black and green dot fluorophores have different frequencies. (d) Recorded image stack, sliced along y-direction, showing the change in the magnitude of the PSFs, associated with individual point objects. (e) 3D image of the 2 fluorophores in the temporal frequency domain after Fourier transforming the image stack (three individual bands can be seen - DC or WF image and positive and negative frequency images; it is only enough to use the positive frequency image, for example, to reconstruct the 3D image of the object). (f) Rescaling the temporal frequency axis into the optical axis by a factor of $\lambda/\Delta\beta(\theta_i)$ and the true 3D image reconstruction.

$$I_{\pm 1}(x, z, \theta_i) = 1 + m\cos\left(2\pi\frac{2}{d}x + 2\pi\frac{z}{\lambda}\beta(\theta_i)\right)$$
$$= 1 + m\cos\left(2\pi\frac{2}{d}x + \phi(z, \theta_i)\right), \qquad (2)$$

where *m* is a modulation depth.

Let us take a closer look at Eq.(2). It is a 2D cosine function describing the spatial distribution of the structured illumination. The first term in the brackets defines the lateral spatial profile of structured light. Regardless of the axial layer z the fringe pattern has the constant period along x-axis: $\Lambda_x = d/2$ (or spatial frequency $f_x = 1/\Lambda_x$) - hence, the term "single-spatial-frequency" interference fringes. The second term inside the brackets in Eq.(2) is the instantaneous phase offset ($\phi(z, \theta_i)$), associated with the single-spatial-frequency fringe pattern. It depends on both instantaneous illumination angle (θ_i) and axial offset of the layer of interest (z). When the instantaneous illumination angle (θ_i) is changed, it alternates the $\beta(\theta_i)$ parameter. Due to the z/λ factor, the amount of change in $\beta(\theta_i)$ parameter will be translated into instantaneous phase offset in each axial layer differently. Altered phase offset will trigger a lateral shift of the fringe pattern. The single-spatial-frequency fringe patterns at axial layers with greater z-coordinate will experience greater lateral shift. Thus, continuously changing the illumination angle, we can make the fringe pattern move across the sample. Hence the name of our system - Moving Fringe SIM. Fig. 3 illustrates the imaging concept of the Moving Fringe SIM.

The fringe pattern is excited by illuminating the grating structure (the reference grating plane is at $z = 0$) with the light coming initially at some incident angle $-\theta_i$. Gradual changes in the incident illumination angle from $-\theta_i$ to $+\theta_i$ make the fringe pattern shift (Fig. 3(a)–(b)). Each of the two fluorescent point-objects at distances $z_1 = 10\lambda$ and $z_2 = 11\lambda$ away from the grating will be traversed by different number of the excitation cycles. Per range of change of $\beta(\theta_i)$ parameter from -0.5 to $+0.5$, the object at axial plane $z_1 = 10\lambda$ will undergo excitation with 10 periods of the structured illumination and the second object at plane $z_2 = 11\lambda$ - with 11 periods (Fig. 3(c)).

The light emitted by both fluorophores in response to the moving fringe excitation pattern is captured by the imaging optics and recorded by the camera (as in Fig. 1). During the image stack acquisition process, the galvo-mirror is driven in a step-and-hold mode. After each increment in illumination angle, the mirror holds its position until a 2D image is captured by camera. The 2D images taken for all incident angles form an image stack.

The image of each fluorescent object is a point spread function (PSF) with lateral coordinates, corresponding to its actual lateral position in space, but the magnitudes of the PSFs vary throughout the image stack, following the excitation pattern. Fig. 3(d) shows a cross-sectional cut of the acquired data matrix along y-direction.

The Fourier transform operation applied to the Moving Fringe system data naturally determines how many excitation cycles have been seen by each fluorophore per given range of incident angles (Fig. 3(e)). Rescaling the temporal frequency axis by a factor of $\lambda/\Delta\beta(\theta_i)$, we convert it into the optical axis, correctly indicating the axial spatial location of the fluorophores - 10 and 11λ away from the grating plane (Fig. 3(f)).

So far, the 3D imaging strategy analysis in this article has not considered the effect of the zeroth diffraction order. However, it can be demonstrated that the interference fringes, produced by the zero order and any of the first orders will have twice the period of the fringes produced by the interference of the two first order beams ($\propto K_g$ not $2K_g$). Hence, while shifting the 3-beam fringe pattern across the sample, the zero order will add another two temporal harmonics to the illumination profile, but the frequency of these harmonics will be twice lower than the frequency of the harmonic produced by the two first orders. Hence, after the Fourier transform, these lower frequency harmonics will not overlap with the harmonic of interest and the effect of the zeroth diffraction order can be safely ignored.

An important advantage of the MF SIM system, compared to the classical SIM method [8], is its independence from the imaging NA. The fringe pattern is projected on the object directly and, hence, the spatial frequencies of the diffraction orders wave vectors, allowed in the system, are not restricted.

III. Axial Resolution in the MF System

As it was shown in the previous section, the axial location of the fluorophore is indicated by the temporal frequency (z) of the intensity signal $I_{\pm 1}(x, z, \theta_i)$. How well the temporal frequencies, corresponding to the different emitters, can be resolved defines the figure of merit of the Moving Fringe system.

A. Axial Resolution With the Fourier Transform

The maximum axial resolution obtainable with the system can be achieved when the variation of $\beta(\theta_i)$ parameter over the

range of the incident illumination angles is maximized.

$$\min(\Delta z_{MF}) = \frac{\lambda}{\max\left[\beta(\theta_{i,\max}) - \beta(\theta_{i,\min})\right]} = \frac{\lambda}{\max\left[2\beta(\theta_{i,\max})\right]}, \tag{3}$$

where we assume a symmetry between $\theta_{i,\max}$ and $\theta_{i,\min}$. Hence, the two diffraction orders, forming the interference pattern, should propagate at right angles at the extrema of the scan, with one beam propagating axially and the other propagating laterally, similar to the depiction in Fig. 2(a),(c).

It is possible to establish the condition for maximizing $\beta(\theta_{i,\max})$ by examining Eq.(1): $\beta(\theta_{i,\max})$ reaches maximum when the minuend is equal to n (i.e. $(\sin(\theta_{i,\max}) + \lambda/d)^2 = 0$) and the subtrahend is equal to zero. Hence, following this argument, it is possible to set the system of equations for the maximum axial resolution in Moving Fringe SIM:

$$\begin{cases} \sqrt{n^2 - \left[\sin\theta_{i,\max} + \frac{\lambda}{d}\right]^2} = n \\ \sqrt{n^2 - \left[\sin\theta_{i,\max} - \frac{\lambda}{d}\right]^2} = 0 \end{cases} \tag{4}$$

Solving it, we find the optimum relationship between the system parameters that maximize the axial resolution:

$$\begin{cases} d_{opt,ax} = \frac{2\lambda}{n} \\ \left|\sin(\theta_{i,\max})\right| = \frac{\lambda}{d_{opt,ax}} \end{cases} \tag{5}$$

and thus, $max(\beta(\theta_{i,\max}))$ becomes equal to n and Eq.(3) can be re-written as:

$$\Delta z_{MF,\min} = \frac{\lambda}{2n}. \tag{6}$$

This is the maximum axial resolution (i.e., the minimum thickness of optical section) the Moving Fringe SIM can achieve if we analyze the data in the frequency domain directly using the Fourier transform.

The figure of merit in evaluating the axial resolving ability of the Moving Fringe SIM is the thickness of its optical section (Δz_{MF}) with respect to that of the WF microscope (Δz_{WF}). Since the resolution of our system is purely dependent on the illumination arrangement and not on the imaging optics, it can deliver a much higher improvement factor than the classical 3D SIM, especially when a low NA lens is used, since the latter has a bigger depth-of-field. The general improvement in axial resolution is given as follows:

$$\frac{\Delta z_{WF}}{\Delta z_{MF}} = \frac{\lambda_{em} n_L}{NA^2} \frac{2n}{\lambda_{ex}}, \tag{7}$$

where NA is the numerical aperture of the imaging lens, n_L is the refractive index of its immersion medium, and λ_{ex} and λ_{em} are the excitation and emission wavelengths respectively. It is important to mention here that although the fluorescent signal is captured at emission wavelength, the illumination profile, which defines the axial resolution in our system is created at λ_{ex}.

Thus, if we compare the thickness of the axial section (thickness of the depth-of-field) of a 1.25 NA oil immersion lens at $\lambda_{em} = 559\,nm$ ($\Delta z_{WF} \approx 545\,nm$) with the maximum achievable resolution in Moving Fringe SIM with optimum settings at $n = 1.33$ and $\lambda_{ex} = 532\,nm$ ($\Delta z_{MF} \approx 200\,nm$), then the improvement factor will be about 2.7. Whereas, if we compare it against the dry 0.65 NA objective ($\Delta z_{WF} \approx 1.33\,\mu m$), improvement factor will be about 6.6.

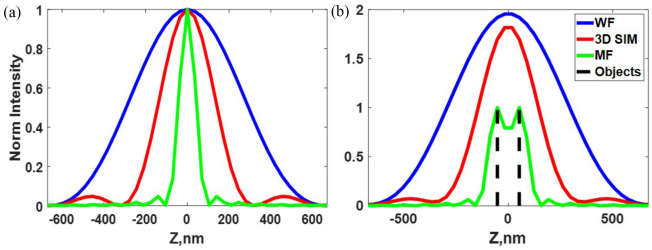

Fig. 4. Axial resolution comparison for NA=1.25 (blue solid curve - WF; red solid curve - 3D SIM; green solid curve - MF). (a) axial cross sections of the PSFs. (b) - comparison of the resolving power for the different systems (axial separation between the objects (black dashed curves) - 100 nm).

Fig. 4(a) shows axial profiles of the PSFs, corresponding to WF, 3D SIM and MF SIM systems, respectively, for the case with 1.25 NA objective lens and Fig. 4(b) compares their resolving abilities for the two point-objects having axial separation of 100 nm.

Hence, the proposed Moving Fringe system can offer a significant improvement in axial resolution compared to the classical 3D SIM. However, in practice, such an improvement would require a complex microscope architecture to address the following two major problems.

The first problem is the maximization of the $\beta(\theta_i)$ parameter variation. From purely theoretical point of view, the range of incident angles is limited by a single condition - the diffraction orders must not become evanescent. Hence, when the air is used as the medium between the grating and sample, the range of the incident angles can be as high as $\pm 30^o$. Filling the space between the grating and the sample with the water (refractive index of 1.33) allows for the range of incident angles extension up to $\pm 41^o$ (both numbers are calculated for the grating with period 1200 gr/mm and $\lambda_{ex} = 532\,nm$). In practice (as in our experimental setup), it is not possible to achieve such high incident angles. The first limiting factor is the galvo-mirror, which can only deflect the light within $\pm 20^o$. The second limiting factor is the telecentric stage (see Fig. 1), where the low NA lenses further limit the range of incident angles. As in our experimental setup, the range of incident angles is limited to $\pm 7^o$.

The second problem is related to the grating itself. Once, propagation angle of the diffraction order approaches 90^o (i.e. evanescent mode) the grating structure will perturb the planar wavefront of such beam, distorting the spatial profile of the interference fringes. Apart from that, the volume where the diffracted orders overlap at high incident angles will tend to zero, making it impossible to assure a proper illumination of the sample across the whole range of the incident angles.

A possible solution for both problems would be to replace the grating structure and the telecentric stage with two independent light sources, but this would lead to an extremely complex mechanical architecture of the microscope illumination unit. An alternative approach, as we demonstrate in this work, is to adopt a

more powerful signal processing tool than the Fourier Transform to analyze the data, which will be discussed in the next section.

B. Axial Resolution With the Minimum-Norm Estimator

As mentioned above, maximizing the variation of the $\beta(\theta_i)$ parameter requires the incident beam to have a wide range of incident angles. In case when only the data from a limited number of angles are available, the data-adaptive spectrum estimation technique, like the Minimum-norm estimator [17], can be used to improve the axial resolution of the proposed Moving Fringe system.

The Minimum-norm algorithm makes use of the autocorrelation matrix of the input data vector to estimate the spectral components of a signal. Define the input data vector ($\boldsymbol{x}(n)$) as a collection of the pixel values at a particular spatial position of the image stack obtained by the CMOS camera. It has the length of N ($0 \leq n \leq N-1$) corresponding to the number of 2D frames acquired. $\boldsymbol{R}_x = E\{\boldsymbol{x}(n)\boldsymbol{x}(n)^H\}$ is the autocorrelation matrix of the input data vector of size $M \times M$ and M is the length of the Minimum-norm window ($M \leq N/2$). In terms of its eigendecomposition it can be written as below:

$$\boldsymbol{R}_x = \sum_{m=1}^{M} \lambda_m \boldsymbol{q}_m \boldsymbol{q}_m^H = \boldsymbol{Q}\boldsymbol{\Lambda}\boldsymbol{Q}^H, \tag{8}$$

where λ_m are the eigenvalues in descending order ($\lambda_1 \leq \lambda_2 \leq \ldots \leq \lambda_M$) and $\boldsymbol{\Lambda}$ is an $M \times M$ diagonal matrix with diagonal values equal to λ_m; q_m are the corresponding eigenvectors, arranged as column vectors in matrix $\boldsymbol{Q}$. Assume there are P fluorescent objects at a particular spatial position but different depths. The data vector $\boldsymbol{x}(n)$ at that spatial position will be composed of P signals of different frequencies. Then the first P eigenvalues can be written as the sum of the signal power in the time window and noise:

$$\lambda_m = M|\alpha_m|^2 + \sigma_\omega^2, \quad m \leq P, \tag{9}$$

where $|\alpha_m|^2$ is the power of the mth signal and σ_ω^2 is the variance of the noise. The remaining eigenvalues are due to the noise only:

$$\lambda_m = \sigma_\omega^2, \quad P < m \leq M. \tag{10}$$

Thus, the autocorrelation matrix can be partitioned into two orthogonal subspaces - signal subspace and noise subspace. Starting from the $M \times (M-P)$ matrix of the noise eigenvectors, $\boldsymbol{Q}_\omega$, we can compute a projection matrix ($\boldsymbol{P}_\omega = \boldsymbol{Q}_{\boldsymbol{\omega}}\boldsymbol{Q}_{\boldsymbol{\omega}}{}^H$) so that any arbitrary vector can be projected to the noise subspace by multiplying with $\boldsymbol{P}_\omega$. A similar projection matrix can be obtained for the signal subspace. The Minimum-norm method seeks to minimize the norm of a vector $\boldsymbol{u}$, which is orthogonal to signal subspace and lies in the same direction of the noise subspace. By minimizing the norm of $\boldsymbol{u}$, we can minimize the spurious peaks in the estimated spectrum [17]. The minimization is subject to the constraint that the first element of $\boldsymbol{u}$ is 1 to ensure the minimum norm solution is not a zero vector. That is,

$$min \quad \| \boldsymbol{u} \|^2 = \boldsymbol{u}^H \boldsymbol{P}_\omega \boldsymbol{u} \quad subject \quad to \quad \sigma_1^H \boldsymbol{u} = 1, \tag{11}$$

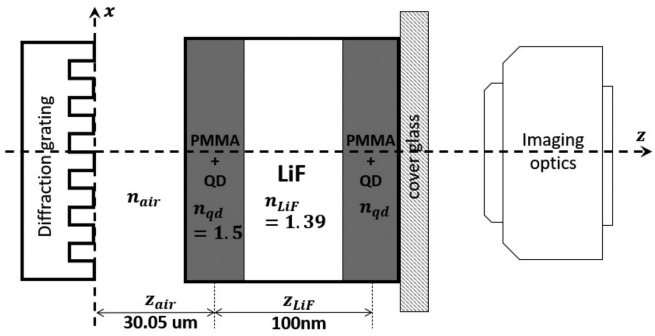

Fig. 5. Simulation setup for the sample with 100 nm separation between the fluorescent layers.

where $\sigma_1 = [1 \quad 0 \quad \ldots \quad 0]^T$ is a constraint vector. The minimization has a close form solution as,

$$\boldsymbol{u}_{MN} = \frac{\boldsymbol{P}_\omega \sigma_1}{\sigma_1^H \boldsymbol{P}_\omega \sigma_1}. \tag{12}$$

A pseudospectrum can be obtained as follows:

$$S_{MN}(\omega) = \frac{1}{|\boldsymbol{v}^H(\omega)\boldsymbol{u}_{mn}|^2}, \tag{13}$$

where $\boldsymbol{v}^H(\omega) = [1 \quad e^{(j\omega)} \quad e^{(j2\omega)} \quad \ldots \quad e^{(j(M-1)\omega)}]^T$. Since $\boldsymbol{u}_{MN}$ lies in the noise subspace, the multiplication with $\boldsymbol{v}^H(\omega)$ theoretically will give a zero value at the signal frequencies. Thus, by checking the peaks in $S_{MN}(\omega)$, we can identify the signal frequencies and thus the positions of the fluorescent objects on the z-axis.

The following subsection evaluates the performance of the Minimum-norm spectrum estimation method in application to the MF system data. As will be shown, the Minimum-norm method significantly improves the axial resolution of the proposed MF SIM system since it can detect the signals even when their spectral peaks are very close to each other. Such resolvability cannot be achieved if we use the traditional spectrum estimation methods, such as the Fourier transform.

Performance of the Minimum-norm method: We use a simulation to illustrate the performance of the Minimum-norm spectrum estimation method in application to the proposed MF SIM system to achieve a 100 nm axial resolution. The simulation studies the fluorescent signals emitted from a sample in the proposed MF SIM system, as shown in Fig. 5. The simulation conditions are as follows: the values of the refractive indices for the fluorescent and neutral layers are 1.5 and 1.39, respectively (the latter index corresponds to the refractive index of Lithium Fluoride). The medium between the grating and sample is free space ($n_m = 1$). 1200 gr/mm grating structure in combination with excitation wavelength of 532 nm caps the maximum range of the incident angles at $\pm 21^o$. The separation between the fluorescent layers is 100 nm. Thus, for a spatial position, there can be at most 2 fluorophores separated by 100 nm.

In all simulation scenarios, the length of the data sequence (N) comprises 1024 points (i.e., we assume 1024 image frames are captured by the CMOS camera), and the window length used in the Minimum-norm method is half of the available data samples

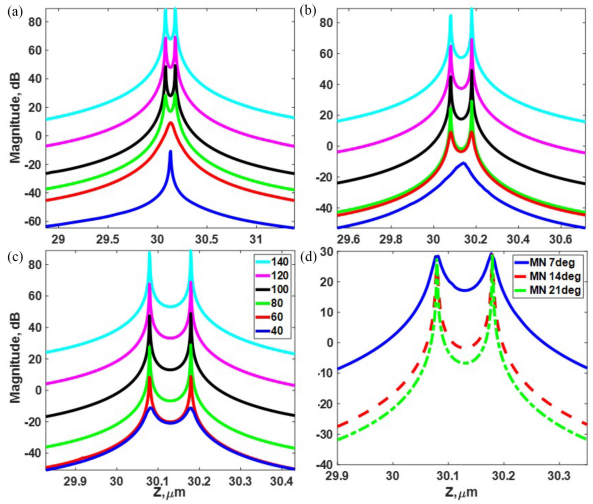

Fig. 6. Comparison of the spectrum estimation methods for the $100\,nm$ axial separation between the fluorescent objects. (a)–(c) % Performance of the Minimum-norm method for the different SNR levels and different range of incident angles ((a) $-\pm 7^o$ – range of angles as in the experiment; (b) $-\pm 14^o$ – median range of angles; (c) $-\pm 21^o$ – maximum range of angles in the free space, respectively; the legend in (c) specifies the SNR). d) Improvement in resolving ability of the Minimum-norm method for the fixed SNR=80 dB for the different ranges of incident angles.

$(M = N/2)$. Since the Minimum-norm method is parametric, we define the noise subspace $(K = M - P)$ to be equal to $7M/8$. Although we know that for the current simulation the number of complex exponentials is equal to 4 (2 real-valued signals, i.e., $P = 2$), we enlarge the signal subspace (minimize the noise subspace) to study the case when the exact number of fluorophores is unknown (as in the experiment) and to check the tolerance of the method to the erroneous guess.

The zero-padding factor was set to 256, i.e., the Fourier transform of the noise-subspace matrix comprises 2^{18} points, as the harmonic models require extremely fine sampling in the frequency domain. Only the portion of the spectrum where the fluorophores are detected is kept. The spectra presented are computed and averaged over 32 noise realizations.

Fig. 6(a)–(c) illustrates the performance of the Minimum-norm method at different signal-to-noise ratio (SNR) levels for the given range of incident angles in order to resolve two fluorescent objects separated by $100\,nm$. As shown in the figures, there are occasions when the two spectral peaks (corresponding to the two fluorescent objects) cannot be resolved. In general, for a given SNR level, the increase in the range of illumination angles improves the resolution dramatically (as illustrated in Fig. 6(d)). However, it will also increase the complexity of the microscope architecture. To reduce the range of illumination angles to, for instance, $\pm 7^o$ (as in our experimental setup), it is necessary to maintain the SNR of not less than 80 dB, as shown in Fig. 6, to resolve two fluorophores with axial separation of $100\,nm$ using the Minimum-norm method.

Fig. 7(a)–(b) shows a comparison between the axial profiles of the reconstructed PSFs as well as the axial resolutions of 3 systems - MF with the Fourier transform (FFT), MF with Minimum-norm, and classical 3D SIM. It can be seen that the

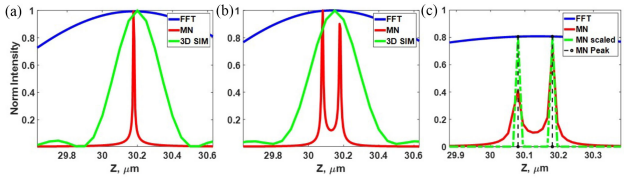

Fig. 7. Axial resolution comparison (blue solid curve - FFT; red solid curve - Minimum-norm ($SNR = 80\,dB$); green solid curve - 3D SIM). (a) axial cross-section of the PSFs. (b) Comparison of the resolving power of different systems (axial separation between the objects - $100\,nm$). (c) Magnitude scaling of the Minimum-norm results using the FFT results as a reference (solid blue curve - FFT result; solid red curve - raw Minimum-norm result; dashed black lines - spectral peaks locations; dashed green curve - Minimum-norm image after magnitude scaling).

proposed MF SIM with the Minimum-norm method gives the sharpest axial profile and accurately indicates the depths of the two fluorophores. On the contrary, the classical 3D SIM method combines the two peaks together and thus cannot identify the positions of the two fluorophores.

Fig. 7(b) indicates a potential complication. While the Minimum-norm method recovers the axial position of the fluorophores correctly, the magnitudes of the spectral peaks, which are supposed to be equal, can be quite different (as also shown in Fig. 7(c)). This is because the Minimum-norm method delivers a pseudospectrum that the magnitude of the spectral peaks does not necessarily correspond to their actual magnitude. While the Minimum-norm method can give an accurate estimation of the spectral peak positions, we propose to use the axial location of the spectral peaks, delivered by the Minimum-norm method, and scale them to match the magnitude generated by another spectrum estimation method that can give a more accurate magnitude. For example, as shown in Fig. 7(c), the magnitudes of the detected spectral peaks are scaled to match the magnitude of the FFT output (black dashed curves and green curve in Fig. 7(c), respectively) to give a better magnitude estimation.

IV. Results

In this section, simulation and experiment results are presented to illustrate the performance of the proposed MF SIM system on axial resolution enhancement in 3D imaging. We first extend the simulation in Section III-B to consider the situation of having multiple fluorophores on the two fluorescent layers. Images of both layers given by different SIM methods are shown and compared. A proof-of-concept experiment is also conducted to test the imaging potential of the proposed system. For completeness, we also explain in the Appendix how the data delivered by the MF SIM can be used for lateral resolution enhancement.

A. Axial Resolution Improvement - Simulation

Recall that our simulation setup contains two layers, $100\,nm$ away from one another, separated by a neutral layer (Fig. 5). Each layer can have many fluorophores located at random spatial positions. Some of them can also be very close to each other spatially. Here, we limit the incident illumination angle to only

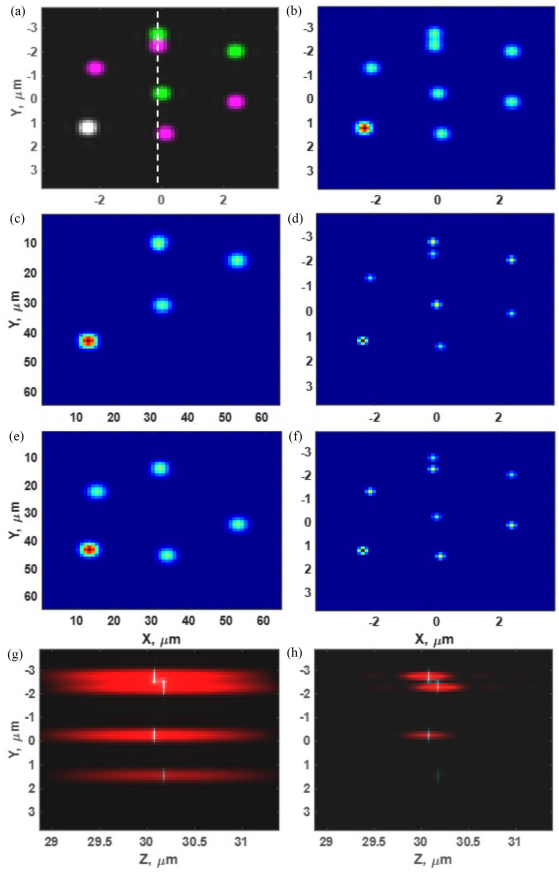

Fig. 8. Simulation of the 2-layer fluorescent sample. (a) Overlay of the WF images of layers 1 and 2, if they were imaged separately (green color - layer 1; magenta color - layer 2; white color - two completely overlapping PSFs in different layers; white dashed line indicates the position of the cross-sectional slice of the 3D images). (b) WF image of the 2-layer sample. (c),(e) Images of the layers 1 and 2 delivered by the MF SIM with the Minimum-norm method, respectively. (d),(f) Images of the layers 1 and 2 delivered by the 3D SIM method, respectively. (g) Composite cross-sectional views of the 3D images, reconstructed using the MF SIM with the Fourier transform (red) and Minimum-norm methods (cyan). (h) Composite cross-sectional views of the 3D images, reconstructed using the 3D SIM (red) and the MF SIM with the Minimum-norm method (cyan).

from $+7$ to -7 degrees with SNR set to 80 dB. The image stack built in simulation consists of 1024 2D images. The whole 3D matrix with the raw data has a dimension of $N_y \times N_x \times N_z$. N_y and N_x define the number of camera pixels in both lateral dimensions; N_z defines the depth of the image stack. For the proposed MF SIM system, we process the image pixels of one spatial position of the image stack at a time, forming the input data sequence for the Minimum-norm method $\boldsymbol{x}(n)$ $(0 \leq n \leq N_z)$.

Fig. 8 shows the results for the simulation with the above conditions. Fig. 8(a) presents a composite WF image of the two fluorescent layers, if they are imaged separately - green and magenta colors mark the fluorophores in layers 1 and 2, respectively; white color marks two emitters, that completely overlap (i.e., two identical objects in each layer with the same lateral coordinates). Fig. 8(b) is the actual WF image of the 2-layer sample.

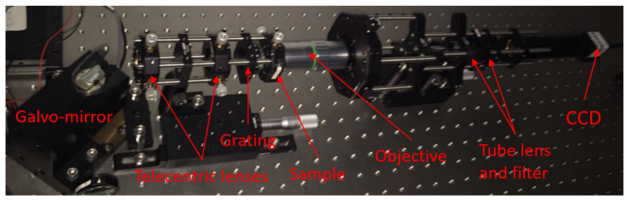

Fig. 9. Moving Fringe SIM system experimental set up.

Comparison of the two fluorescent layers images reconstructed using Minimum-norm (Fig. 8(c),(e)) and the classical 3D SIM methods (Fig. 8(d),(f)) shows a significant amount of the overlap between the axial layers in the case of the 3D SIM. The axial resolution of the 3D SIM method is not high enough to fully resolve the objects separated by $100\,nm$ axially. On the contrary, the proposed MF SIM with the Minimum-norm method can separate the layers with much higher confidence. It should be noted that the objective of MF SIM is to enhance the axial resolution, not the lateral resolution. So one can find in Fig. 8(c),(e) that the lateral resolution of the image is the same as before. As a future work, we will show in Appendix how the MF SIM data can also be used to enhance the lateral resolution.

Fig. 8(g) shows an overlay of the cross-sectional views of the 3D images reconstructed using the Fourier transform (red) and Minimum-norm method (cyan). The 3D images are sliced along the white dashed line in Fig. 8(a). Similarly, Fig. 8(h) shows an overlay of the cross-sectional views of the 3D images reconstructed using the 3D SIM (red) and Minimum-norm method (cyan). The 3D images were sliced along the same white dashed line in Fig. 8(a). One can clearly see the improvement in axial resolution achieved by the proposed MF SIM with the Minimum-norm over the classical 3D SIM.

B. Axial Resolution Improvement - Experiment

The potential of MF SIM with the Minimum-norm method for delivering a 3D image with enhanced axial resolution is further verified via experimental results. Fig. 9 depicts the actual experimental setup of the MF SIM, corresponding to the schematic shown in 1.

During the image stack acquisition process, the actual position of the galvo-mirror had been measured via a feedback channel; and prior to the signal processing, the phase jitter in the measured intensity signals was reduced via interpolation. The image stack formed during the experiment comprises 1024 frames taken for the range of incident angles from -7 to $+7$ degrees.

In order to test the MF SIM performance, we use a sample with $250\,nm$-thick fluorescent layer, made of CdSe/ZnS quantum dots (QD) solution mixed with nonfluorescent polymethyl methacrylate dissolved in toluene and spin coated on a cover glass. Although the QD are distributed on the surface of the cover glass, they still have small axial variations in the layer. The objective of this experiment is to find out if the proposed MF SIM system can identify their axial variations.

Fig. 10 shows the processing results for the $250\,nm$-thick fluorescent sample. Fig. 10(a) illustrates the CCD frames captured

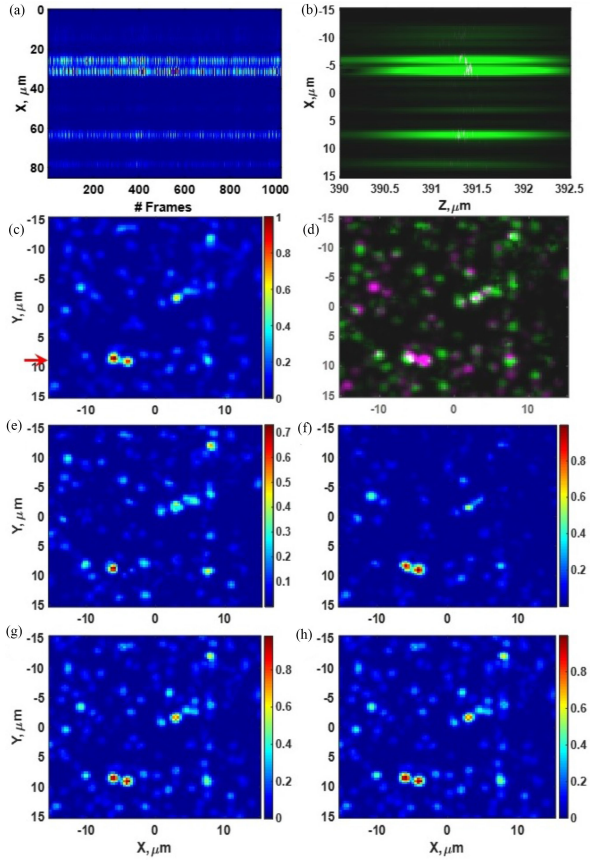

Fig. 10. 3D reconstruction of the volumetric sample processed with different methods. (a) CCD frames captured during the image acquisition process (3D data matrix was sliced along x-axis, at the position, indicated by the red arrow in (c)). (b) Overlay of the axial cross-sections of the 3D images (sliced along x-axis, at the position, indicated by the red arrow in (c)) reconstructed by the MF SIM system with the FFT method (green color) and with the Minimum-norm method (magenta color). (c) WF image (red arrow indicates the position where the 3D data matrix was sliced). (d) Overlay of the two sub-layer images given by the proposed MF SIM system with the Minimum-norm method (green color - sub-layer 1; magenta color - sub-layer 2; white color - overlapping objects from different sub-layers). (e),(f) Individual sub-layer images given by the proposed MF SIM system with the Minimum-norm method. (g),(h) Individual sub-layer images given by the proposed MF SIM system with the FFT method.

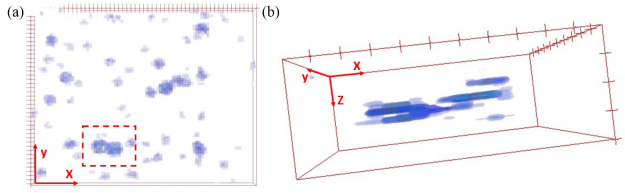

Fig. 11. Volumetric reconstruction of the results delivered by the MF SIM system with Minimum-norm method. (a) 3D image in $x-y$ axes. (b) 3D image in $x-y-z$ axes (for clarity, only the portion of the image inside the red dotted rectangle in (a) is displayed).

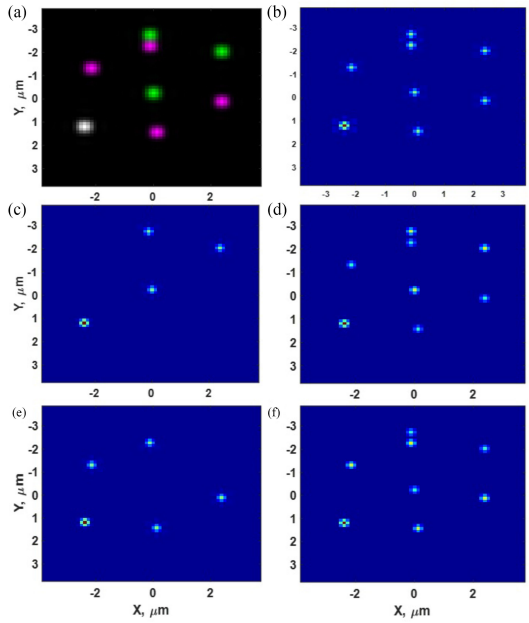

Fig. 12. Multidimensional resolution improvement using the reconstructed 2D SIM image as a magnitude mask for the Minimum-norm image of the 2-layer simulated sample. (a) Composite image of layers 1 and 2, delivered by the MF SIM with the Minimum-norm method (green color - layer 1; magenta color - layer 2; white color - overlapping PSFs). (b) Reconstructed 2D SIM image with lateral resolution improvement. (c),(e) Images of Layer 1 and Layer 2, delivered by the MF SIM with the Minimum-norm method and the 2D SIM magnitude mask applied. (d),(f) Images of Layer 1 and Layer 2, delivered by the classical 3D SIM method.

by the MF system during the image acquisition process (the raw data matrix was sliced at the position indicated by the red arrow in Fig. 10(c), along x-axis). Overlay of the axial cross-sections of the 3D images, reconstructed using the MF SIM system with the FFT method (green colour) and with the Minimum-norm method (magenta color) is shown in Fig. 10(b). It can be seen that a dramatic improvement in the accuracy of the axial location of the fluorophores is achieved when the MF SIM system is used with the Minimum-norm method. Fig. 10(c) displays the WF image of the sample. It does not contain any axial information. All QD at different axial positions are shown together. The intensity of the image is controlled by the concentration of QD. By using the proposed MF SIM system with the Minimum-norm method, we can divide the 250 nm-thick fluorescent layer into 50 optical sections, each 5 nm thick. Such fine sampling of the optical axis allows us to build images of fluorescent sub-layers by accumulating desired number of axial slices. Fig. 10(d) shows the overlay of the two sub-layer images that are built up by accumulating 25 slices for each (green color - sub-layer 1; magenta color - sub-layer 2). Fig. 10(e),(f) show the two sub-layers individually. It can be seen that some objects that appear in one layer are not found in the other layer. It shows that the proposed MF SIM system with the Minimum-norm method can resolve fluorescent objects separated by about 100 nm axially. Fig. 10(g),(h) show the individual images for the same sub-layers reconstructed when FFT is used as the signal processing tool for the MF SIM system. Due to the limited range of incident angles ($\pm 7^o$), the axial resolution of the system is limited if we just use the Fourier transform to estimate the spectrum of the data vectors (Fig. 10(b)). We have explained the problem in Section III-A. One can see in Fig. 10(g),(h) that the images of the two sub-layers are almost identical to one another and the WF image. The result

indicates the important role of the Minimum-norm method in the proposed MF SIM system.

Fig. 11 shows the volumetric image of the $250\,nm$-thick fluorescent sample, created with the software ImageJ [19], using the results delivered by the MF SIM with the Minimum-norm method. Fig. 11(a) presents a volumetric image in $x-y$ axes in transparent mode, where an overlay of the fluorophores from all axial layers can be observed. Fig. 11(b) shows a portion of the volumetric image (inside the red dotted rectangle in Fig. 11(a)) in $x-y-z$ axes. This image illustrates how the fluorophores are distributed in the sample along z-axis.

Conclusion and future work

In this paper, a novel super-resolution 3D imaging system based on moving fringe structured light illumination (MF SIM) is proposed. We have shown that the proposed MF SIM can bypass the limiting effect of the imaging optics in the classical 3D SIM methods. The axial resolution of MF SIM is determined only by the illumination mechanism thus, potentially, a larger improvement factor in the axial resolution can be achieved over the classical 3D SIM. However, we have also demonstrated that, in practice, the actual axial resolution can be limited by the range of incident angles. To solve the problem, we propose to use the Minimum-norm method for estimating the spectrum of the acquired data vectors. We leverage the high resolvability of the Minimum-norm method to improve the axial resolution of the proposed MF SIM system. Our simulation results have illustrated its ability to precisely sense the actual locations of the fluorescent objects and how it outperforms the classical 3D SIM method. A $100\,nm$ axial resolution can be achieved even for the case of having a limited range of incident angles, as long as a high SNR is maintained for the fluorescent signals acquired by the Moving Fringe system. For demonstrating the feasibility of the proposed MF SIM system, a proof-of-concept experiment has been presented. Since the Minimum-norm method can deliver a very fine sampling of the optical axis, it allows for the custom thickness of the optical sections in the reconstructed 3D image. A simple and rapid hardware implementation along with fine axial sectioning allows the proposed MF SIM system to compete, axial resolution-wise, with far more complex designs, such as 4Pi or I ^{5} M [20].

Although this article largely focuses on axial resolution improvement, we believe that the data acquired by the proposed Moving Fringe imaging system can also be used for simultaneous lateral resolution enhancement. One of the possible ways of simultaneous multidimensional resolution improvement is briefly discussed in the Appendix. It will be the focus of our future research work related to Moving Fringe structured light illumination systems.

Appendix
Moving Fringe SIM in Application to Lateral Resolution Improvement - Simulation

Apart from axial resolution improvement, the MF SIM system data can also be used for lateral resolution enhancement. Although in the MF SIM system we project the fringe pattern axially to the sample, it can be shown that, laterally, the sample will also be illuminated by a fringe pattern. It means that the traditional 2D SIM method can be used to enhance the lateral resolution using the MF SIM data. However, the proposed MF SIM uses a fringe pattern of single orientation, i.e., 0^o, for axial resolution enhancement. It will only allow us to improve the lateral resolution in a single direction along the x-coordinate. In order to achieve a uniform lateral resolution improvement, two more scans with fringe patterns of 60^o and 120^o spatial orientation should be added. The 2D SIM image with enhanced lateral resolution can be used as a magnitude mask for the Minimum-norm method to set the magnitude of the spectral peaks for axial resolution enhancement. As a result, the images delivered by the Minimum-norm and 2D SIM method can be combined towards a super-resolved 3D image.

A simulation similar to that in Section IV-A is carried out to verify the idea. Fig. 12(a),(b) shows the image with axial resolution improvement delivered by the proposed MF SIM with the Minimum-norm method and the corresponding 2D SIM image, respectively. Fig. 12(c),(e) depicts the final super-resolution images of layers 1 and 2, respectively, obtained via combining these two methods together. Fig. 12(d),(f) shows the reference images of layers 1 and 2 obtained with the classical 3D SIM method (calculated numerically using the specified dimensions of the PSF, reported in [8]). The result shows that the proposed method can improve both the lateral and axial resolutions simultaneously. It outperforms the classical 3D SIM particularly on the axial resolution that objects in different axial layers can be clearly separated out. The investigation of the principles allowing a seamless and error-proof way of combining the axially and laterally super-resolved images will be the focus of our further research work.

Acknowledgment

The authors would like to thank Dr. Shen Hong for her help in sample preparation.

References

[1] R. Heintzmann and C. G. Cremer, "Laterally modulated excitation microscopy: Improvement of resolution by using a diffraction grating," *SPIE Proc.*, vol. 3568, pp. 185–195, 1999.

[2] M. G. L. Gustafsson, "Surpassing the lateral resolution limit by a factor of two using structured illumination microscopy," *J. Microsc.*, vol. 198, pp. 82–87, 2000.

[3] J. T. Frohn, H. F. Knapp, and A. Stemmer, "True optical resolution beyond the rayleigh limit achieved by standing wave illumination," *Proc. Nat. Acad. Sci. USA*, vol. 97, pp. 7232–7236, 2000.

[4] M. G. L. Gustafsson, D. A. Agard, and J. W. Sedat, "Doubling the lateral resolution of wide-field fluorescence microscopy using structured illumination," *SPIE Proc.*, vol. 3919, pp. 141–150, 2000.

[5] M. A. A. Neil, R. Juskaitis, and T. Wilson, "Method of obtaining optical sectioning by using structured light in a conventional microscope," *Opt. Lett.*, vol. 22, pp. 1905–1907, 1997.

[6] M. Neil, R. Juskaitis, and T. Wilson, "Real time 3D fluorescence microscopy by two beam interference illumination," *Opt. Commun.*, vol. 153, pp. 1–4, 1998.

[7] B. Bailey, D. L. Farkas, D. L. Taylor, and F. Lanni, "Enhancement of axial resolution in fluorescence microscopy by standing-wave illumination," *Lett. Nature*, vol. 366, pp. 44–48, 1993.

[8] M. G. L. Gustafsson *et al.*, "Three-dimensional resolution doubling in wide-field fluorescence microscopy by structured illumination," *Biophysical J.*, vol. 94, pp. 4957–4970, 2008.
[9] L. Shao, B. Isaac, S. Uzawa, D. Agard, J. Sedat, and M. Gustafsson, "I5s: Wide-field light microscopy with 100-nm-scale resolution in three dimensions," *Biophysical J.*, vol. 94, pp. 4971–4983, 2008.
[10] J. R. Choi and D. Kim, "Enhanced image reconstruction of three-dimensional fluorescent assays by subtractive structured-light illumination microscopy," *J. Opt. Soc. Amer. A., Optics, Image Sci., Vis.*, vol. 29, pp. 2165–2173, 2012.
[11] M. Shaw, L. Zajiczek, and K. O'Holleran, "High speed structured illumination microscopy in optically thick samples," *Methods*, vol. 88, pp. 11–19, 2015.
[12] K. Wicker, O. Mandula, G. Best, R. Fiolka, and R. Heintzmann, "Jointly super-resolved and optically sectioned bayesian reconstruction method for structured illumination microscopy," *Opt. Exp.*, vol. 21, pp. 2032–2049, 2013.
[13] Z. Cai, X. Liu, X. Peng, and B. Z. Gao, "Universal phase-depth mapping in a structured light field," *Appl. Opt.*, vol. 57, pp. A26–A32, 2018.
[14] H. Choi, D. Wadduwage, P. T. Matsudaira, and P. T. C. So, "Depth resolved hyperspectral imaging spectrometer based on structured light illumination and fourier transform interferometry," *Biomed. Opt. Exp.*, vol. 5, pp. 3494–3507, 2014.
[15] B.-J. Chang *et al.*, "Two-beam interference lattice lightsheet for structured illumination microscopy," *J. Phys. D: Appl. Phys.*, vol. 53, 2019, Art. no. 044005.
[16] C. W. See, C.-J. Chuang, S. Liu, and M. G. Somekh, "Proximity projection grating structured light microscopy," *Appl. Opt.*, vol. 49, pp. 6570–6576, 2010.
[17] D. M. Manolakis, V. K. Ingle, and S. M. Kogon, *Statistical and Adaptive Signal Processing*. London, U.K.: Artech House, 2005.
[18] J. W. Goodman, *Introduction to Fourier Optics*. New York, NY, USA: McGraw-Hill, 1996.
[19] C. T. Rueden *et al.*, "ImageJ2: ImageJ for the next generation of scientific image data," *BMC Bioinf.*, vol. 18, no. 1, pp. 1–26, 2017.
[20] W. Liu *et al.*, "Breaking the axial diffraction limit: A guide to axial super-resolution fluorescence microscopy," *Laser Photon. Rev.*, vol. 12, no. 8, 2018, Art. no. 1700333.